GEORG-AUGUST-UNIVERSITÄT
GÖTTINGEN

Fakultät für Physik
Friedrich-Hund-Platz 1
37077 Göttingen

http://advanced-lab-course.physik.uni-goettingen.de

Advanced Lab Course I, II

Solid State and Materials Physics (M.Phy.1401, M.Phy.1402)

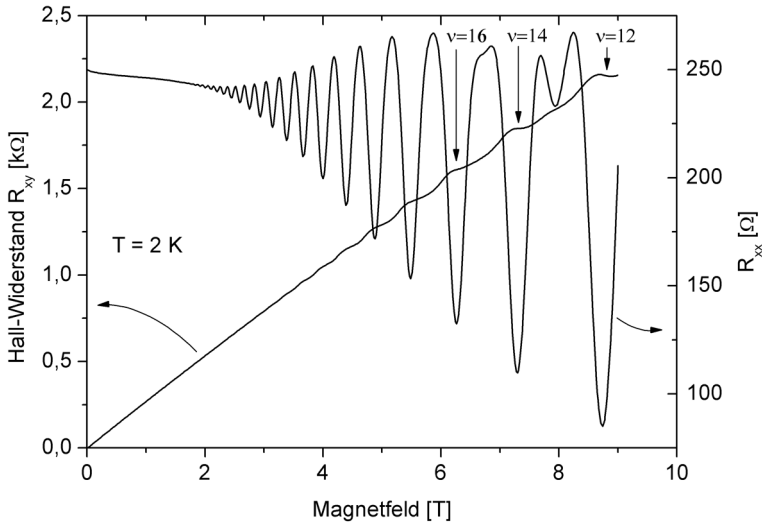

Lab Course Instructions to FM.QHE

Quantum-Hall-Effect

FM.QHE
Version 2024.01/E

IV. Physikalisches Institut
J. Malindretos

Zusammenfassung

Die elektrische Charakterisierung eines Halbleiters beginnt oft mit der Bestimmung der Ladungsträgerkonzentration und der Beweglichkeit durch eine Hall-Effekt Messung. Aus der Temperaturabhängigkeit dieser Größen lassen sich weitere Rückschlüsse auf Aktivierungsenergien oder auf die beteiligten Streumechanismen ziehen. So weisen zweidimensionale Elektronengase (2DEG), die beispielsweise an AlGaN/GaN Grenzflächen entstehen können, einen grundlegend anderen Temperaturverlauf der Beweglichkeit auf als Volumen-Halbleiter, da die Streuung an ionisierten Störstellen unterdrückt wird. Daraus resultieren in der Regel insbesondere bei tiefen Temperaturen sehr hohe Beweglichkeiten und große freie Weglängen.

Wenn ein hochbewegliches 2DEG bei tiefen Temperaturen und bei hinreichend großen Magnetfeldern gemessen wird, so bilden sich Plateaus in der Magnetfeldabhängigkeit des Hall-Widerstandes aus, die auf einen makroskopischen Quantenzustand im System zurückzuführen sind. Für die Entdeckung dieses „Quanten-Hall-Effekts“ erhielt Klaus von Klitzing 1985 den Nobelpreis.

In dem Versuch wird zunächst der klassische Hall-Effekt in Abhängigkeit von der Temperatur an einem vorstrukturierten 2DEG gemessen. Der gut zugängliche Aufbau besteht dabei aus einem Durchfluss-Kryostaten, einem Elektromagneten und der Meßelektronik. Auf diese Weise bietet der Versuch einen Einblick in das Experimentieren bei tiefen Temperaturen und vermittelt grundlegende Techniken elektrischer Messungen. Die gewonnenen Daten werden anschließend einer Messung des Quanten-Hall-Effekts gegenübergestellt, die aus einem Aufbau mit höheren Magnetfeldern stammt. Beide Datensätze sollen im Rahmen des Versuches analysiert und ausgewertet werden.

Summary

Carrier concentration and mobility are essential parameters in the electrical characterisation of semiconductor materials. They can be readily determined by Hall-Effect and resistivity measurements. Moreover, the temperature dependence of these quantities can be used to extract further information about the material, such as activation energy or relevant scattering mechanisms. For example, two-dimensional electron gases (2DEGs) exhibit a fundamentally differnet temperature dependence of the mobility as compared to bulk material, due to the absence of scattering from ionised impurities in the 2DEG channel.

Two-dimensional electron gases with high mobility develop plateaus in the Hall resistance at high magnetic fields. For the discovery of this so called Quantum-Hall-Effect sKlaus von Klitzing was awarded the Nobel prize in 1985.

In this lab course, classical Hall-Effect measurements will be performed on various semiconductor heterostructures at first. The experimental setup mainly consists of a continous flow cryostat, an electro-magnet (capable of generating magnetic fields up to about 1 T) and the electronic measurement system. In this way, basic techniques of electrical characterization and low-temperature physics are demonstrated. The results will be analysed in detail, together with the data set of a Quantum-Hall-Effect measurement obtained for the very same sample in a different setup (with a superconducting magnet).

1 Physical principles

1.1 The electrical conductivity of metals

More than 100 years ago, Drude described metallic conductivity using the assumption of an ideal elecrton gas in the solid. The dynamics of an electron with charge $q = -e$ in an external electrical field E is then described by the classical equation of motion

$$m\dot{v} + \frac{m}{\tau}v_D = -eE \; . \tag{1}$$

The dissipative effect of scattering is accounted for by the friction term, where v_D is the so-called drift velocity. When the external field is switched off, the velocity v will relax exponentially to the thermal velocity with the time constant τ, which is called relaxation time. For the stationary case ($\dot{v} = 0$) one has

$$v_D = -\frac{e\tau}{m}E \tag{2}$$

and hence the current density j in the direction of the electric field is

$$j = -env_D = ne\mu E \; . \tag{3}$$

Here n is the volume density of all free electrons and the mobility μ is defined as the proportionality constant between the drift velocity and the external field. In the Drude model, the electrical conductivity is therefore

$$\sigma = j/E = ne\mu \; , \tag{4}$$

where $\mu = e\tau/m$. Note however, that in this simple model all free electrons contribute to the current. This view is in contradiction to the Pauli principle. For the Fermi gas this forbids electrons well below the Fermi level from acquiring small amounts of energy, since all neighboring higher energy states are occupied.

To relate the material-specific conductivity to atomically determined features of the band structure, one has to sum up the contributions of all electrons with different wave vectors. This means that one has to integrate over all states in the first Brillouin zone (not carried out in detail here)

$$\mathbf{j} = -\frac{1}{8\pi^3}\; e \int_{1st\; BZ} d\mathbf{k}\; v(\mathbf{k}) f(\mathbf{k}) \; , \tag{5}$$

where $f(\mathbf{k})$ is the occupation probability for a state $\mathbf{k}$, given by the Boltzmann equation. Restricting to linear effects in an external field, i.e. Ohm's law, one ends up with the same expressions for the conductivity σ and the mobility μ like those of the Drude model, with the difference that the free electron mass m is replaced by the effective mass $m*$ and that the relaxation time τ is that of electrons at the Fermi level $\tau(E_F)$. The total concentration n of electrons appears only because of the formal integration over k-space and not because all carriers contribute to charge transport [1].

1.2 The electrical conductivity of semiconductors

In a semiconductor there is an energy gap, that separates the highest filled band (valence band) from the lowest empty band (conduction band). Because of the Pauli principle,

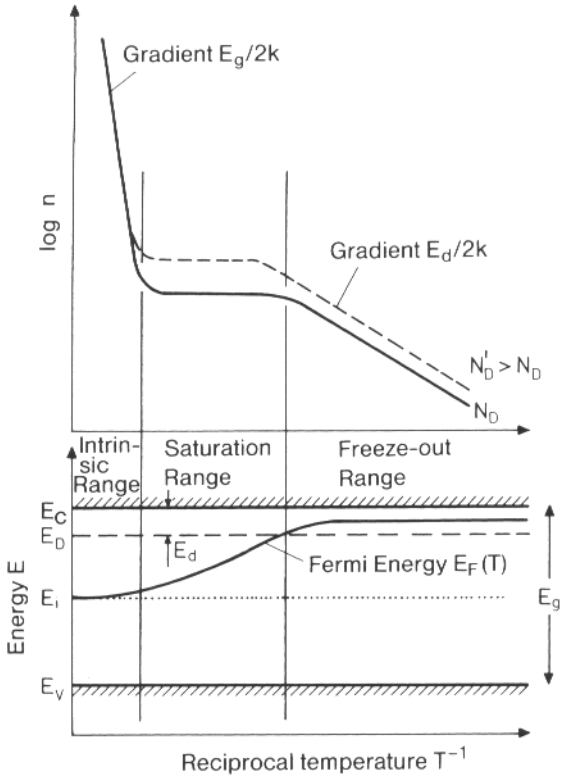

Figure 1: Qualitative temperature dependence of the concentration n of electrons in the conduction band of an n-type semiconductor for two different donor concentrations $N_D' > N_D$. The width of the forbidden band is E_g and E_d is the ionization energy of the donors. The qualitative temperature dependence of the Fermi energy $E_F(T)$ is shown in the lower part of the figure. E_C and E_V are the lower edge of the conduction band and the upper edge of the valance band, respectively. E_D is the position of the donor levels and E_i is the Fermi energy of an intrinsic semiconductor. Taken from [1].

only carriers in the conduction band can participate in electrical transport phenomena. However, the intrinsic carrier concentration n_i due to thermal activation over the bandgap, which is usually of the order of electron volts, is not nearly large enough to yield current densities necessary for practical semiconductor devices.

By doping, i.e. the addition of electrically active impurities, the concentration n of free electrons in the conduction band (or the concentration p of free holes in the valence band) can be increased by many orders of magnitude compared to the intrinsic case. The temperature dependence of the electron concentration n is schematically shown in Fig. 1.

For a general treatment of the electrical conductivity in a semiconductor, one has to consider both the electrons in the lower conduction band region with a concentration n and a mobility μ_n and the holes at the upper valence band edge with a concentration p and a mobility μ_p. The current density j in an isotropic semiconductor is therefore

$$j = e(n\mu_n + p\mu_p) \; . \tag{6}$$

In contrast to a metal, where only electrons at the Fermi edge need to be considered, the mobilities μ_n and μ_p in a semiconductor are average values for the electron and hole occupied states in the lower conduction band and upper valence band, respectively. In non-degenerate semiconductors, Fermi statistics can be approximated by Boltzmann

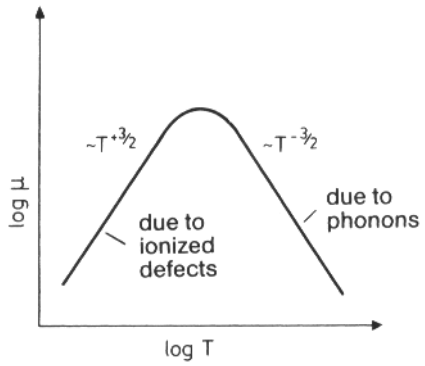

Figure 2: Schematic temperature dependence of the mobility μ for a semiconductor in which scattering from phonons and charged impurities occurs. Taken from [1].

statistics in this region. Within the framework of this approximation, the averaging, which will not be carried out in more detail, yields the following expression

$$\mu_n = \frac{e}{m_n^*} \frac{\langle \tau(\mathbf{k}) v^2(\mathbf{k}) \rangle}{\langle v^2(\mathbf{k}) \rangle} \ . \tag{7}$$

Instead of deriving a rigorous solution of the Boltzmann equation and an exact further treatment of Eq. (7), we restrict ourselves to a more qualitative discussion of the scattering processes undergone by the free carriers in a semiconductor. In this respect, electrons and holes behave in a qualitatively similar manner. After considerable simplification, Eq. (7) yields a proportionality between the mobility and the relaxation time ($\mu \propto \tau$), which holds exactly in the case of metals. Because τ is proportional to the average time between collisions, it follows that

$$\frac{1}{\tau} \propto \langle v \rangle \Sigma \ , \tag{8}$$

where Σ represents the scattering cross section for electrons and holes at a scattering center.

The two main scattering mechanisms are phonon scattering and defect scattering. Assuming that these mechanisms are independent of each other and keeping in mind that the scattering probability is inversely proportional to the free time of flight, it follows that

$$\frac{1}{\tau} = \frac{1}{\tau_{ph}} + \frac{1}{\tau_{def}} \ , \tag{9}$$

where τ_{ph} and τ_{def} are the average times between scattering from phonons and from defects, respectively. Estimating the cross sections Σ_{ph} and Σ_{def} one arrives at $\mu_{ph} \sim T^{-3/2}$ and $\mu_{def} \sim T^{3/2}$. The reciprocal of the total mobility is given by the sum of the reciprocal mobilities. The resulting temperature dependence of the mobility in a bulk semiconductor is depicted in Fig. 2. Note however, that the situation can be much more complicated if further scattering mechanisms are involved, e.g. piezoelectric scattering or scattering from optical phonons.

1.3 Two-dimensional electron gases

A sequence of two different semiconductor layers grown epitaxially onto each other is called a heterostructure. In the vicinity of the interface, the free carriers will rearrange

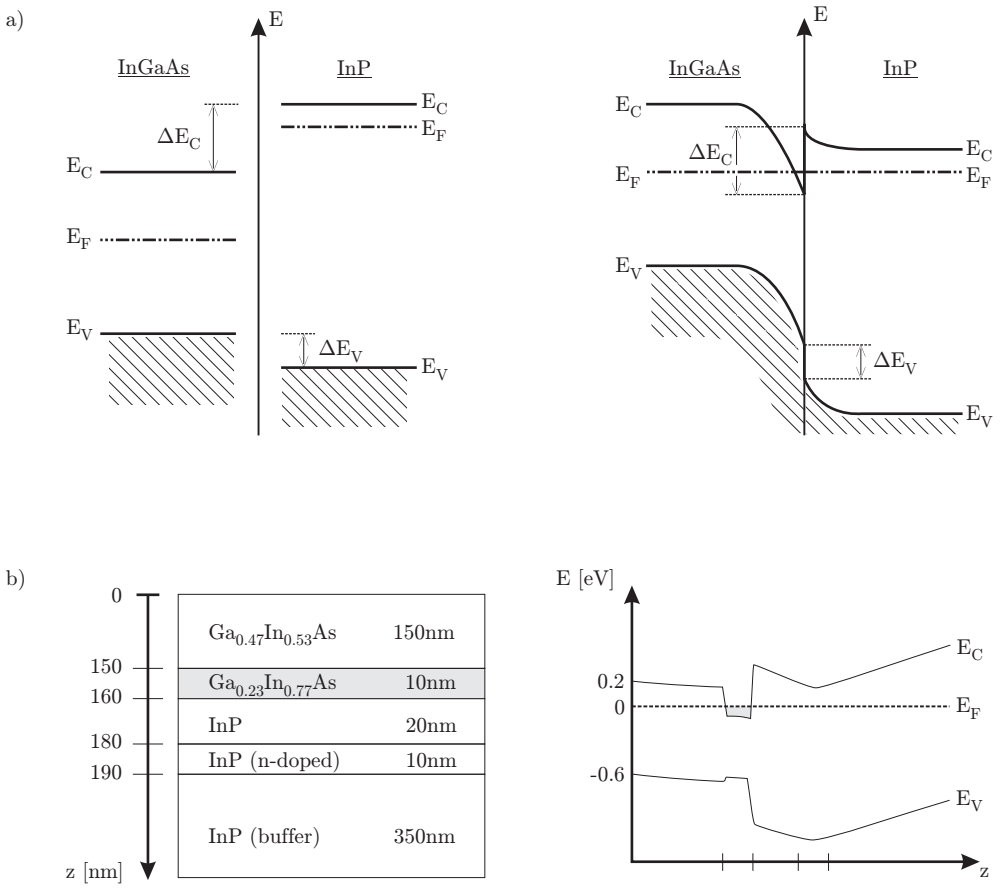

Figure 3: Schematic bandstructure of a heterostructure before and after thermal equilibrium (a). In (b) a typical layer sequence and a self-consistently calculated bandprofile of a realistic InP/InGaAs heterostructure are shown. An undoped InP spacer layer further separates the 2DEG from the ionized donors in the doped InP layer. The top $Ga_{0.47}In_{0.53}As$ layer is lattice matched to the InP substrate.

until the Fermi levels on both sides have aligned in thermal equilibrium. Away from the interface, the band discontinuities of the valence band ΔE_V and the conduction band ΔE_C as well as the position of the Fermi level with respect to the conduction or valence band remain unchanged. This implies that the energetic bands are bent in a narrow region around the interface. In this way, a potential well can form in the semiconductor with the smaller band gap, in which electrons can accumulate (Fig. 3a). This electron enrichment layer is typically about (5 to 10) nm in width (dependent on the doping of the semiconductor layers) and is called two-dimensional electron gas (2DEG), because the free electrons are confined here in the narrow triangular potential well and can move freely only in the direction parallel to the heterostructure. An example of a realistic 2DEG layer structure is shown in Fig. 3b.

The charge of the high concentration of free electrons in the two-dimensional electron gas is compensated by a depletion region in the opposite layer, where the ionized donors are located. These donors have given one of their valence electrons into the energetically favorable potential well. In this way, high concentration of free electrons is spatially separated from the ionized impurities. Defect scattering, which is the main contribution to the electrical resistance at low temperatures, does not play a vital role in a two-dimensional

electron gas. In this way, the mobility at low temperatures is strongly enhanced (Fig. 4).

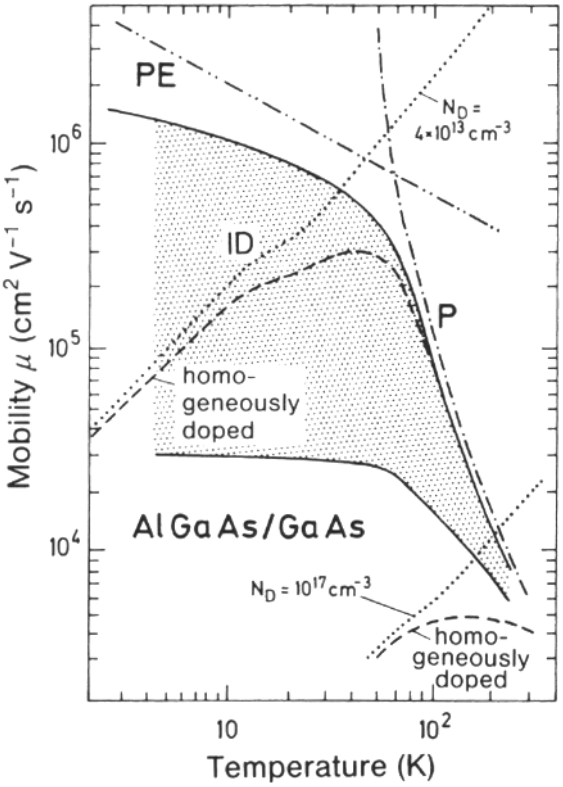

Figure 4: Temperature dependence of the electronic mobility in a two-dimensional electron gas. The shaded region represents a great many experimental data. For comparison the mobility curves of homogeniously doped GaAs with two differnt donor concentrations are shown (dashed). The limiting values of the mobility are determined by the following mechanisms: scattering from ionized impurities (ID), phonon scattering (P) and piezoelectric scattering (PE). Taken from [1].

1.4 The classical Hall effect

Hall effect measurements are nowadays a standard method to electrically characterize a semiconductor [2]. The majority carrier type and concentration as well as their mobility can be determined. In this section the Hall effect for electrons (n-type semiconductor) is described. Analogous equations hold for the case of holes (p-type semiconductor).

We can consider a rectangular shaped sample of single carrier type conduction with four contacts at the edges. An electric field $\mathbf{E}_x$ is applied resulting in a current flow $\mathbf{j}_x$ through the sample. According to the picture shown in Fig. 5 the electrons are moving from the front contact to the back contact, whereas holes would travel in the opposite direction. A uniform magnetic induction $\mathbf{B}_z$ is applied perpendicular to the current. So the carriers flowing in the semiconductor will experience a Lorentz-force bending their trajectories, and they will build up on one side of the sample. An electric field starts to built up along the y direction, which counteracts the Lorentz-force. After a short time equilibrium is reached and no current is flowing in the y-direction $I_y = 0$. This voltage is called the *Hall voltage*, V_H. For developing a simple expression for the Hall voltage, we assume within the Drude relaxation approximation that all the conduction carriers have the same drift

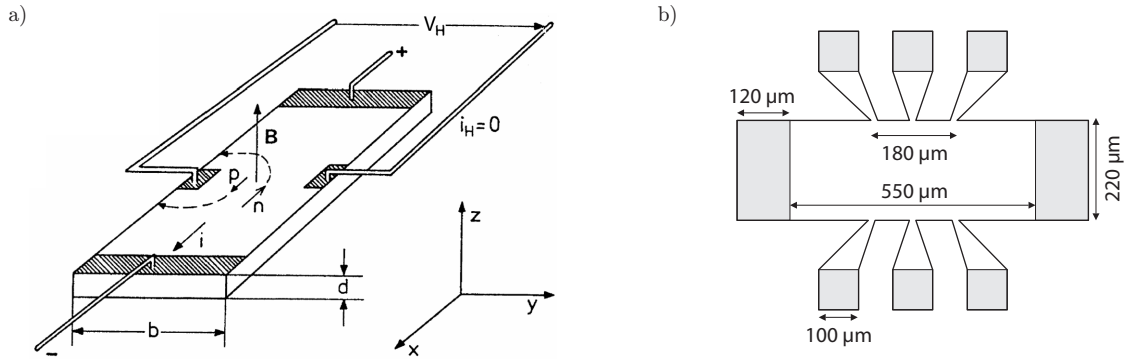

Figure 5: (a) Sign convention and terminology for a rectangular Hall sample. Taken from [1]. (b) Layout and dimensions of the bar-type samples used for the measurement.

velocity $\mathbf{v}_d$ and the same relaxation time τ_c. In this case the Lorentz-force that acts on the carriers can be expressed like

$$\mathbf{F}_L = q \cdot (\mathbf{v}_d \times \mathbf{B}) \tag{10}$$

where q is the elementary charge ($q = -e$ for electrons and $q = +e$ for holes). So, the Lorentz-force points in the negative y-direction for both, electrons and holes, and its norm is given by

$$F_L = e \cdot v_D \; B_z$$

The carriers are attracted to the left side (see Fig. 5), where they cause an electric field, given by

$$\mathbf{F}_E = q \cdot \mathbf{E} \tag{11}$$

This force points in the positive y-direction and opposes the force $\mathbf{F}_L$ caused by the magnetic field. Its norm amounts to

$$F_E = e \cdot E_y$$

For n-type conductivity, the electrical field points in the negative y-direction. In steady state, the sum of all forces is equal to zero

$$\mathbf{F}_L + \mathbf{F}_E = 0 \quad \Rightarrow \quad e \cdot v_D \; B_z = e \; E_y \tag{12}$$

Expressing the drift velocity using the current density $j = env_D$, where n is the bulk electron concentration, and writing the electrical field as $E_y = V_H/b$, we arrive at

$$\frac{j \cdot B_z}{e \cdot n} = \frac{V_H}{b}$$

Making use of $j = I/(b \cdot d)$ we finally obtain an expression that allows to determine the carrier concentration from the measurement of the Hall factor R_H

$$R_H \equiv \frac{V_H \cdot d}{I \cdot B_z} = \frac{1}{e \cdot n} \tag{13}$$

If the Hall voltage V_H is negative, the conduction is caused by electrons and if it is positive, the conduction is caused by holes ($n \to p$).

In order to be able to calculate the mobility of the carriers according to Eq. (4), one also has to know the conductivity $\sigma = j/E_x$. Then the mobility is given by

$$\mu = \frac{\sigma}{e \; n} = \frac{I}{V_x \cdot e \; n} \cdot \frac{l_x}{b \; d} \tag{14}$$

where V_x is the voltage drop over a length l_x along the direction of the current.

1.5 The van der Pauw method

According to the work of L. J. van der Pauw [3] it is possible to measure the specific resistivity and the Hall effect on an arbitrarily shaped sample. A special preparation of the sample is not necessary. The measured sample only has to fulfill the following requirements:

- the contacts are positioned on the sample edge
- the contacts are small compared to the sample size
- the thickness of the sample is constant
- the surface introduces an uninterrupted coherent area

1.5.1 Resistivity measurement

According to the contact designation shown in Fig. 6, the van der Pauw resistivity can be defined as:

$$R_{2134} = \frac{V_{34}}{I_{21}} \,, \tag{15}$$

where the current flows through the contacts 2 and 1, and the voltage is measured between the contacts 3 and 4. It can be shown that the conductivity is given by:

$$\sigma = \frac{ln2}{\pi d} \cdot \frac{2}{R_{2134} + R_{3241}} \left[f(Q) \right]^{-1} \qquad \text{with} \quad Q = \frac{R_{2134}}{R_{3241}} \tag{16}$$

where f is a correction factor for the geometrical asymmetry (not for material anisotropy or inhomogeneity), that depends on the symmetry factor Q, defined as ratio of the resistivities for two pairs with a common contact.

For an *ideal square* sample, the symmetry factor is $Q = 1$. Good sample preparation will routinely achieve a value for Q less than 1.2, although values of Q up to 1.5 will still yield reasonable measurements. Values of $Q > 1.5$ are usually a result of badly defined van der Pauw patterns, non-Ohmic contacts or anisotropic samples. Note that bar-type or bridge-shaped specimen might be more suitable for anisotropic samples. *Rectangular* samples will naturally have values of $Q > 1$ so that for these samples the symmetry factor cannot be used to monitor sample quality.

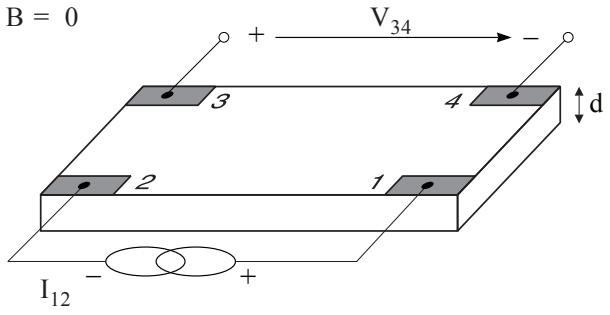

Figure 6: Van der Pauw arrangement for measuring the conductivity of an arbitrarily shaped sample.

The correction factor f is normally obtained by reference to graphs. However, if the asymmetry is not too large ($Q < 10$), the following approximation can be used:

$$f \simeq 1 - 0.34657\, A - 0.09236\, A^2 \qquad \text{with} \quad A = \left[\frac{Q-1}{Q+1}\right]^2 \tag{17}$$

To reduce the influence of any non-symmetry of the sample, it is useful to average the conductivity over all possible permutations of the four contacts and over both current directions (forward and reverse). In terms of the specific resistivity $\rho = \sigma^{-1}$ one ends up with

$$\rho = \frac{\pi d}{ln2} \cdot \frac{1}{8} \left\{ \begin{array}{r} \left(R_{2134} - R_{1234} + R_{3241} - R_{2341}\right) f_A + \\ \left(R_{4312} - R_{3412} + R_{1423} - R_{4123}\right) f_B \end{array} \right\} \tag{18}$$

where the correction factors $f_A(A_A)$ and $f_B(A_B)$ are given according to the definition in Eq. (17), and the symmetry factors Q_A and Q_B account also for the reverse current direction

$$Q_A = \frac{R_{2134} - R_{1234}}{R_{3241} - R_{2341}} \qquad \text{and} \qquad Q_B = \frac{R_{4312} - R_{3412}}{R_{1423} - R_{4123}} \tag{19}$$

1.5.2 Hall factor

For the Hall effect measurement the current flows through the sample and on the remaining two contacts the Hall voltage is measured perpendicular to the current (Fig. 7). Again it is useful to average over the current and magnetic field polarities. Ideally, the Hall voltage is zero if no magnetic field is applied. In reality however, this voltage is non-zero due to sample inhomogeneities. Accordingly,the following magneto-resistivities are defined:

$$\begin{array}{l} R_1^{B+} = \frac{1}{2}\left\{(R_{1324}(B+) - R_{1324}(0) + R_{3142}(B+) - R_{3142}(0)\right\} \\ R_2^{B+} = \frac{1}{2}\left\{(R_{4213}(B+) - R_{4213}(0) + R_{2431}(B+) - R_{2431}(0)\right\} \\ R_1^{B-} = \frac{1}{2}\left\{(R_{1324}(B-) - R_{1324}(0) + R_{3142}(B-) - R_{3142}(0)\right\} \\ R_2^{B-} = \frac{1}{2}\left\{(R_{4213}(B-) - R_{4213}(0) + R_{2431}(B-) - R_{2431}(0)\right\} \end{array}$$

The averaged magneto-resistivity is given by

$$R_{avg} = \frac{1}{4}\left\{R_1^{B+} + R_2^{B+} - R_1^{B-} - R_2^{B-}\right\}$$

and the Hall factor can be computed by analogy with Eq. (13)

$$R_H = \frac{1}{8}\,\frac{d}{B_z} \cdot \left\{ \begin{array}{r} \left(R_{3142}(B+) - R_{1342}(B+) + R_{1342}(B-) - R_{3142}(B-)\right) + \\ \left(R_{4213}(B+) - R_{2413}(B+) + R_{2413}(B-) - R_{4213}(B-)\right) \end{array} \right\} \tag{20}$$

The carrier concentration can then be calculated by

$$n = \frac{1}{e \cdot R_H} \tag{21}$$

and the carrier mobility can be determined by

$$\mu = \frac{\sigma}{e \cdot n} = \frac{|R_H|}{\rho} \quad . \tag{22}$$

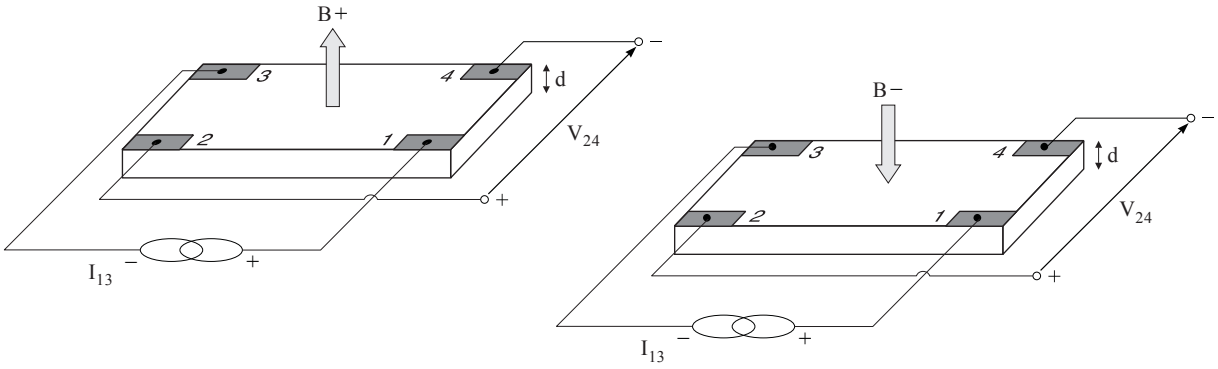

Figure 7: Van der Pauw arrangement for measuring the Hall factor of an arbitrary shaped sample.

1.6 The integral quantum Hall effect

The magnetotransport properties of a two-dimensional electron gas in a high magnetic field, which is applied perpendicular to the plane of the quantum film, are surprisingly different from the case of small magnetic fields discussed in Sec. 1.4. In 1980, K. von Klitzing and coworkers [9] discovered a quantization of the Hall resistance R_H in strong magnetic fields ($\omega_c \tau \geq 1$) with plateaus at

$$R_H = \rho_{xy}(B) = \frac{1}{\nu_n} \frac{h}{e^2} \qquad \text{with} \quad \nu_n = 1, 2, 3, ... \in \mathbb{N} \tag{23}$$

where h is Planck's constant and ν_n is an integer. The resistance values of the Hall plateaus are universal, in the sense that they depend only on fundamental constants and not on any material parameters.

The quantum Hall effect is closely connected to the magneto-oscillation of the longitudinal resistivity $\rho_{xx}(B)$, known as *Shubnikov-de Haas oscillations*. In the regions of quantized Hall resistance, ρ_{xx} drops to zero, while peaks in the longitudinal resistivity are observed, whenever there is a jump in the Hall resistivity ρ_{xy}, i.e when the filling factor changes.

The common origin of both effects is the *Landau quantization* in strong magnetic fields. The energy levels of the two-dimensional electron gas condensate into a finite number of discrete energy levels. In order to explain the integral quantum Hall effect two concepts are employed [5]. In the edge-state model, the quantum Hall effect is interpreted in terms of one-dimensional current channels along the edges of the sample. Another important notion is the fact that disorder induced scattering leads to broadening of the Landau levels and to a significant density of states between two ideal Landau levels. However, only the states around the energy positions of the ideal Landau levels are extended. The other states are localized in space and do not contribute to the current flow.

In ultra high mobility samples, even fractional filling factors can be observed [10]. This phenomenon is a many-particle effect and its discussion is beyond the scope of this laboratory course.

1.6.1 Landau quantization

The single particle Schroedinger equation for a two-diimensional electron gas in a magnetic field B reads

$$\left[\frac{(\mathbf{p}+e\mathbf{A})^2}{2m^*}+V(z)\right]\phi(\mathbf{r})=E\phi(\mathbf{r}) \tag{24}$$

where $\mathbf{A}$ denotes the vector potential, such that $\mathbf{B}=\nabla\times\mathbf{A}$, and $(-e)$ is the charge of the electron. Since the magnetic field is assumed to be perpendicular to the plane of the two-dimensional electron gas, the z-direction can be treated separately, leading to a quantized energy E_z, which is the conduction band bottom of the 2DEG. For mathematical simplicity, the vector potential can be chosen in the Landau gauge, $\mathbf{A}=(-B\,y,0,0)$, leaving the xy-Hamiltonian

$$H_{xy}=\frac{1}{2m^*}\,\left[(p_x-e\,B\,y)^2+p_y^2\right] \tag{25}$$

With the ansatz

$$\phi(x,y)=\psi(y)\cdot\exp(ik_x x) \tag{26}$$

a one-dimensional Schroedinger equation in the y-direction is obtained,

$$\left[-\frac{\hbar^2}{2m^*}\frac{\partial^2}{\partial y^2}+\frac{\hbar^2k_x^2}{2m^*}-\frac{\hbar k_x eBy}{m^*}+\frac{e^2B^2y^2}{2m^*}\right]\,\psi(y)=(E-E_z)\psi(y) \tag{27}$$

while plane waves are the eigenfunctions in the x-direction of the separated Hamiltonian. The Schroedinger equation for the y-direction can be mapped onto the harmonic oscillator equation

$$\left[-\frac{\hbar^2}{2m^*}\frac{\partial^2}{\partial\xi^2}+\frac{1}{2}m^*\omega_c^2\xi^2\right]\,u(\xi)=Eu(\xi)\qquad\text{with}\quad\xi\to y-\frac{\hbar k_x}{m^*\omega_c} \tag{28}$$

where $\omega_c=eB/m^*$ is the cyclotron frequency of the electron in the magnetic field. The eigenfunctions of the xy-Hamiltonian are thus plane waves in x-direction (with k_x quantized as a consequence of periodic boundary conditions), multiplied with Hermite polynomials in the y-direction centered at $y_k=\hbar k_x/(eB)$. A more detailed description of this calculation can be found in [11, 6].

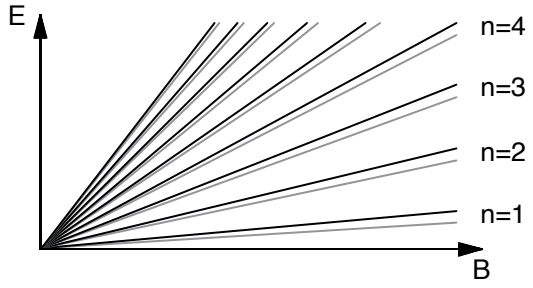

Figure 8: Energy of the first Landau levels as a function of the applied magnetic field. The size of the Zeeman splitting has been exaggerated for graphical reasons.

The corresponding energy eigenvalues are

$$E_{ns}=E_z+\hbar\omega_c\left(n-\frac{1}{2}\right)+sg\,\mu_B\,B\qquad\text{with}\quad n=1,2,3,... \tag{29}$$

The last term with denotes the additional contribution of the Zeeman energy, where $s = \pm 1/2$ is the electron spin and g is the Landé factor.

Besides spin and valley degeneracies, the degeneracy of each energy level is given by the numer of allowed wave numbers in x-direction. The states of energy E_{ns} form the n-th Landau level. In order to determine the degenerac of a Landau level, one can use the fact that the integrated density of states is independent of the magnetic field. Hence, the density of states of an ideal 2DEG in a strong perpendicular magnetic field reads

$$D(E) = \eta \, \frac{m^*}{2\pi\hbar^2} \, \hbar\omega_c \, \delta(E - E_{ns}) = \eta \, \frac{1}{2\pi \, \ell_B^2} \, \delta(E - E_{ns}) \tag{30}$$

where η is the spin and valley degeneracy and $\ell_B = \sqrt{\hbar/eB}$ is called the magnetic length, which corresponds to the width of the ground state in a quantizing magnetic field.

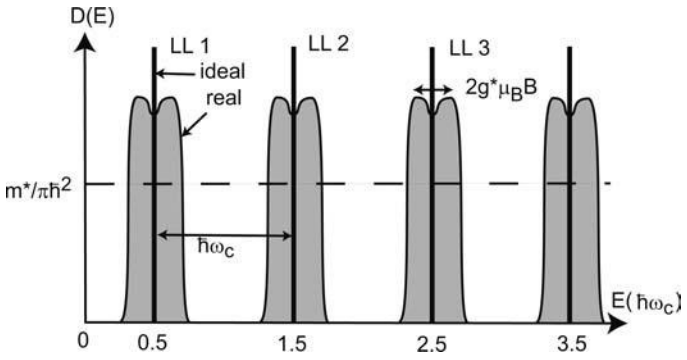

Figure 9: Ideal and real densities of states of a Landau-quantized 2DEG that is spin degenerate at $B = 0$. The δ functions broaden due to fluctuations of the conduction band bottom, while the spin degeneracy is lifted for $B > 0$, and a Zeeman doublet results for non-zero effective g-factors. Taken from [6].

Thus the number of states per unit area in a Landau level is given by

$$n_L = \eta \, \frac{eB}{h} \tag{31}$$

At low and intermediate values of the magnetic field, the Zeeman splitting can often be neglected, so that $\eta = 2$ due to the resulting spin degeneracy. Note that the energetic position as well as the degeneracy of the Landau levels depend on the magnetic field.

Another useful quantity is the filling factor ν, which is defined as the (fractional) number of Landau levels occupied with electrons. For a 2DEG with a sheet carrier density n_{2D}, the filling factor is obtained by

$$\nu = \frac{n_{2D}}{n_L} \tag{32}$$

Hence, a total of $\nu_n = \lceil \nu \rceil$ Landau levels (with spin degeneracy η) contain electrons.

1.6.2 Edge channel model

In order to understand the causes for the existence of plateaus in the Hall resistance as well as for the observation of Shubnikov-de Haas oscillations, a more profound consideration

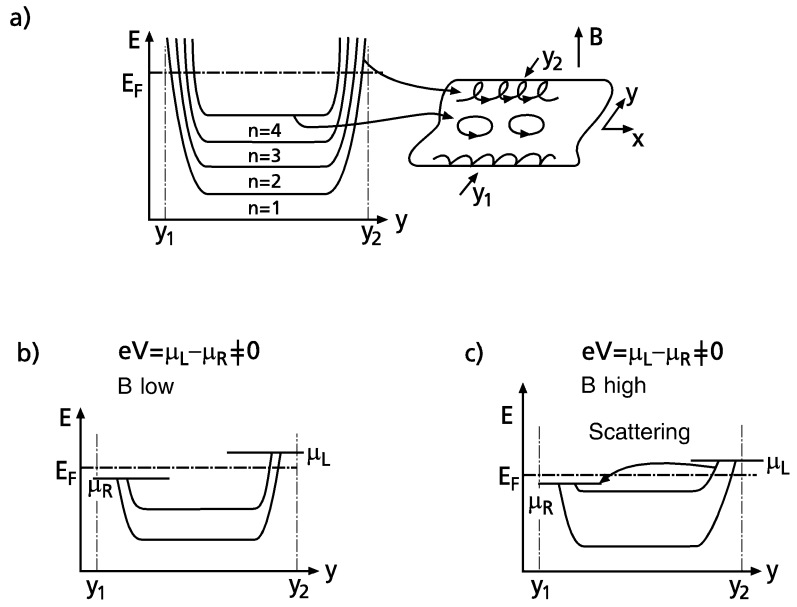

Figure 10: Explanation of the edge channels for electrons when a magnetic field B is applied perpendicular to the plane of a 2DEG. (a) A strong magnetic field B perpendicular to the 2DEG causes quantization of the electronic states into Landau levels (n = 1,2, ...), which correspond to closed cyclotron orbits in the interior of the sample. At the sample boundaries y_1 and y_2 orbiting is interrupted by elastic reflection from the surface. The increased spatial confinement entails a strong enhancement of the energy of the Landau levels, which eventually cross the Fermi energy E_F. (b) Under the condition of ballistic current flow the chemical potentials μ_R and μ_L of the right and left edge channels are different and determine the potentials of the corresponding right and left contacts. (c) With increasing magnetic field B the splitting between the Landau levels increases, while the upper Landau level approaches the Fermi level E_F. Electronic states near E_F in the interior of the sample become available for scattering processes and the left and right edge channels communicate by these scattering processes. Taken from [1].

of the transport in a 2DEG in the presence of a magnetic field is necessary [1]. In a strong magnetic field, electrons in the 2DEG are forced into cyclotron orbits. Undisturbed, closed orbits, however, are possible only in the interior of the sample.

In that case, the orbital energies are those of the undisturbed Landau levels. Electrons near the boundaries of the sample on the other hand are hindered to complete a full cyclotron orbit. In the simplest case of an elastic mirror reflection at the boundary the electron path becomes a sequence of partial circles (skipping orbits). The combination of cyclotron orbits and surface scattering in the skipping orbits amounts to an additional spatial confinement of the electrons. By virtue of the uncertainty principle, a stronger confinement is equivalent to a higher kinetic energy. Near the boundaries of the sample the energies of the Landau level are therefore bent upwards and eventually even cross the Fermi level E_F at y_1 and y_2 near the sample surface (Fig. 10a). Crossing the Fermi level means that one has metallic conduction. Thus, a Landau level that cannot contribute to the electrical conductance in the bulk of the material (since its energy is deep below the Fermi level) does contribute to the conductance at the surface, in the so-called *edge channels*. The edge channels possess a further important property. Transport in these states is quasi-ballistic, even in macroscopic samples containing impurities. When a carrier in an edge channel is scattered from a defect, its trajectory is redirected into the forward

direction by the Lorentz force of the strong magnetic field. The total current in the forward direction is therefore not reduced by the presence of impurities and transport in edge channels is therefore quasi-ballistic, i.e. without resistance, regardless of the presence of impurities.

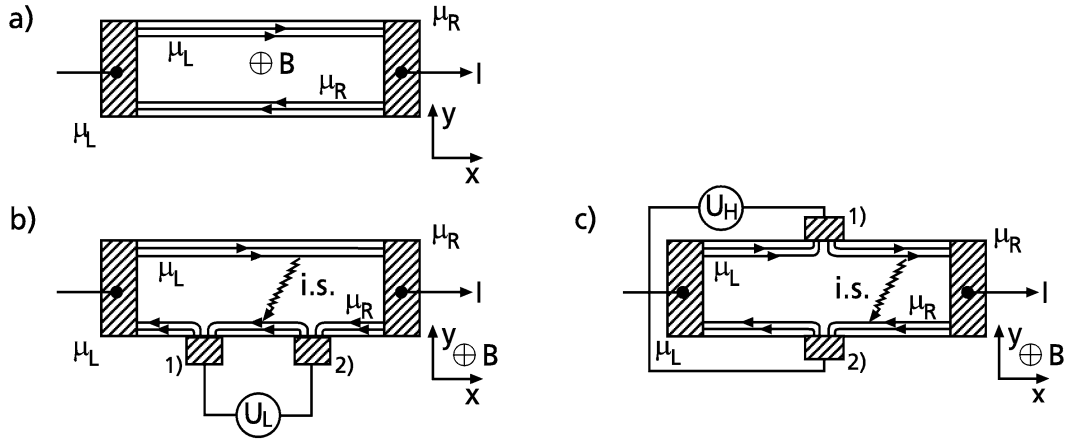

Figure 11: (a) Ballistic electron transport in edge channels that are generated by quantization in a spatially limited 2DEG due to a strong perpendicular magnetic field B. Under the assumption of negligible inelastic scattering between left (L) and right (R) channels the chemical potentials μ_L and μ_R of the left and right channels equal those of the left and right electrical contacts. (b) Conduction through edge channels in a 2DEG in the presence of two electrical contacts 1) and 2) for measuring the Shubnikov-de Haas oscillations in a strong magnetic field. Inelastic scattering (i.s.) between left and right channels causes a potential difference between the contacts. (c) Conduction through edge channels in a 2DEG with two opposite contacts 1) and 2) for measuring the quantum Hall effect. Taken from [1].

The two edge channels on either side are electrically isolated from each other provided that the Landau levels in the interior of the sample are more than a few k_BT below the Fermi energy E_F. Because of the quasi-ballistic transport in the channels, electrons within one channel are at the same potential. For an electron current flow from left to right this potential is the potential μ_L of the left contact, while electrons in the right ""backwards"" edge channels are at the potential of the right contact μ_R (Fig. 11). The difference in the potential is the applied voltage multiplied by the electron charge

$$\mu_L - \mu_R = eV \tag{33}$$

The net electric current carried by the left and right (one-dimensional) edge channels is the diference between the contributions from both contacts [1, 5]:

$$I = \sum_n \int_{\mu_R}^{\mu_L} e\, D_n^{(1D)}(E)\, v_n(E)\, \mathrm{d}E \tag{34}$$

The sum runs over all occupied Landau levels n, which cross E_F as edge channels, $D_n^{(1D)}$ is the one-dimensional density of states of the n-th edge channel, while v_n is the electron velocity within this channel. The n-th edge channel thus contributes to the current an amount

$$I_n = \frac{e}{h}\,(\mu_L - \mu_R) = \frac{e^2}{h} V \tag{35}$$

The quantum Hall efect is measured as the resistance between left and right edge channels via two contacts perpendicular to the current flow (Fig. 11c). According to Eq. 35 each channel contributes an amount of e^2/h to the total conductance, i.e. h/e^2 to the Hall resistance. This is exactly the quantum by which the resistance is stepwise enhanced each time a further Landau level crosses the Fermi energy and is thus depleted of electrons. The Shubnikov-de Haas efect is explained in a similar way. In this case, the magneto-resistance is measured along the path of the current via two contacts arranged along the edge channels (Fig. 11b). As long as the Landau levels in the interior of the sample are sufciently far away from E_F, no voltage drop occurs, because of the ballistic transport. At a particular magnetic field one of the Landau levels in the interior of the sample reaches the Fermi level E_F and electronic states for scattering between the left and right edge channel become available. Scattering between the forth and back channels induces a resistance along the channel direction. Hence, at these particular magnetic fields a peak-like increase of the resistance is observed. In this interpretation, both quantum Hall efect and Shubnikov-de Haas oscillations are attributed to quasi-one-dimensional carrier transport in edge channels [1, 12].

1.6.3 Disorder

The above discussion shows that the longitudinal resistance can be extremely small if the electrochemical potentials μ_1 and μ_2 were located between bulk Landau levels. This requires that the equilibrium Fermi energy E_F must be located between the Landau levels since at low bias $\mu_1 \sim \mu_2 \sim E_F$. However, this is extremely unlikely since the density of states in this region is very small. A slight change in the electron density would cause a large shift in the Fermi energy. The Fermi energy thus tends to be pinned to energies where the density of states is high.

From this point of view one would expect the Fermi energy to be pinned to one Landau level or another, where the density of states is high. If this were true then the low resistance condition discussed above would never be observed since the Fermi energy would never be located between two Landau levels. This is not a problem in narrow conductors where the edge states provide a significant density of states between the Landau levels. But in wide conductors the edge states represent a negligible fraction of the total density of states.

However, it is believed that in practice the density of states between two Landau levels is quite significant because real samples have potential fluctuations leading to the formation of localized states. This can be understood by noting that potential fluctuations in the interior of the sample lead to the formation of local equipotential contours that close on themselves. Since cyclotron orbits drift along equipotential contours they get stuck at these spots forming localized states. These states do not contribute to the current flow but they help stabilize the Fermi energy between Landau levels by providing a respectable density of states between Landau levels [5].

2 Technical description

The sample is bonded into a standard 14-pin DIP chip carrier and mounted into a continuous flow cryostat that provides quick refrigeration between 2 K and 300 K. The cryostat

is located between the poles (100 mm diameter) of a water cooled electromagnet, that is capable of creating magnetic fields up to 1 T at a pole separation of 40 mm.

2.1 Electrical components for AC measurements

A sketch of the AC measurement setup is shown in Fig. 12. An adjustable current source drives a current through the sample and the voltage drop between two further contacts is measured and amplified with a differential amplifier (with a gain of up to 500). The current source can be controlled with a DC input voltage and a superimposed AC signal, which is attenuated by a factor of up to 10^3.

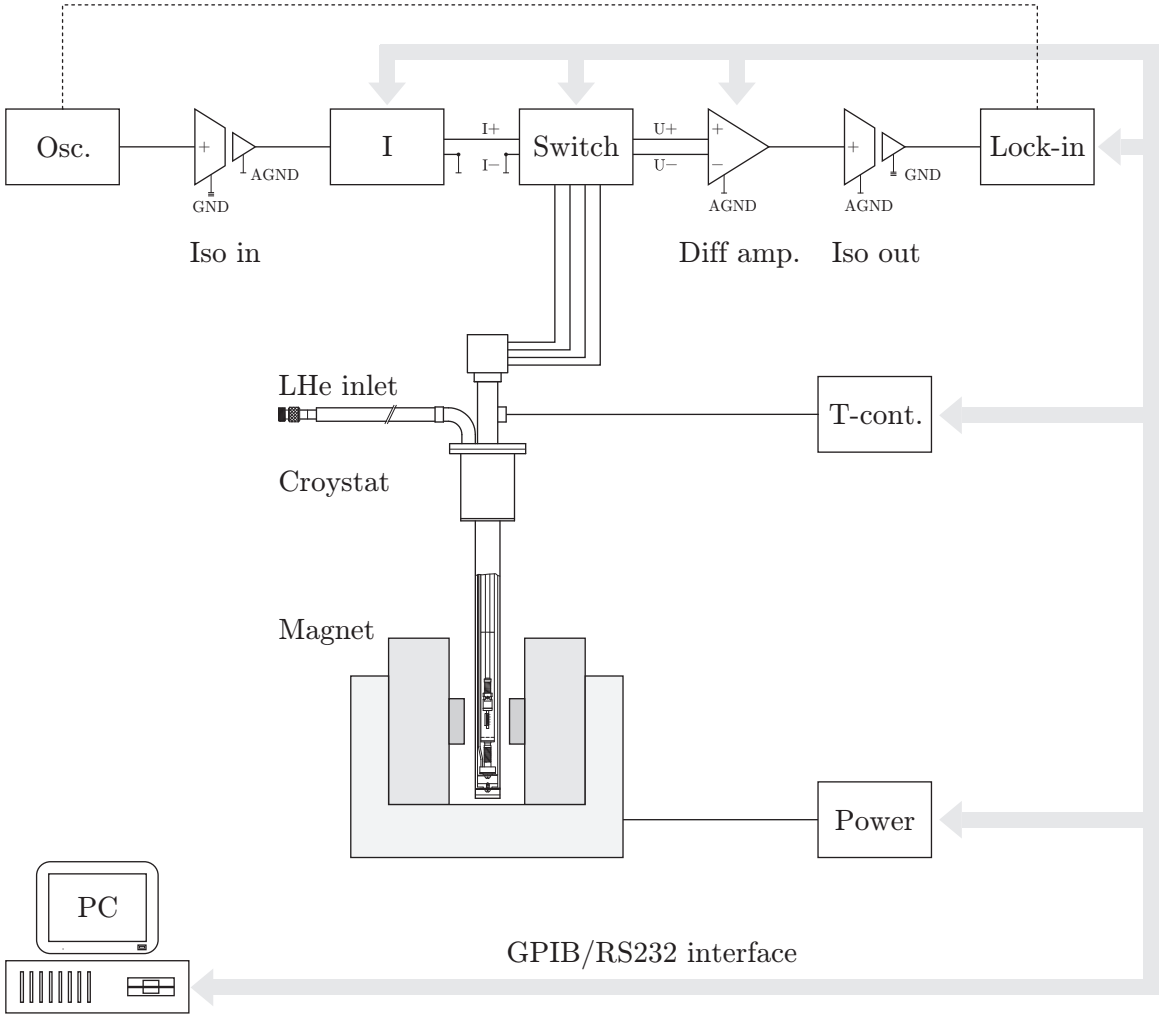

Figure 12: Setup of the Hall system for AC measurements. Isolation amplifiers and lock-in technique are used to reduce noise. A switch box is used to connect the current input and the voltage output to the sample leads. All components can be addressed by a computer over a GPIB or an RS232 interface.

The input lines (current) and the output lines (voltage) are connected to the sample via a matrix switch that is built up with reed-relays. In this way, the current can be applied between any two contacts of the sample without the need to rewire the lines. This can be particularly useful when making van der Pauw measurements (Sec. 1.5).

To reduce noise and thus to improve the accuracy of the measurement, isolation amplifiers (each with a gain of 10) and lock-in technique are employed. The former help to prevent the formation of a ground-loop, which may cause an inaccurate representation of the measured signal. The latter is used in general to measure small signals buried in noise (not white noise) and to eliminate the 50 Hz or 60 Hz noise. To achieve this, a small AC current I_{osc} is superimposed on the measurement current and phase locked with the lock-in amplifier. The lock-in amplifier is equipped with an internal oscillator whose frequency may be adjusted over a wide range and which may be used exactly for this purpose (by connecting it to the input of the current source). In the present case, another advantage of using an AC measurement setup is the elimination of thermoelectric voltages which are a common source of error in low voltage measurements (e.g. the measurement of Hall voltages in samples with high carrier concentrations).

The lock-in amplifier evaluates only the signal component at the oscillator frequency. A Taylor expansion of the measurement signal demonstrates the principle

$$U(I) = U(I_{dc}) + \underbrace{\left|\frac{dU}{dI}\right|_{I_{dc}} i_{osz}}_{\text{lock-in measurement}} \cdot \cos\omega t + \frac{1}{4}\left|\frac{d^2U}{dI^2}\right|_{I_{dc}} {i_{osz}}^2 \cdot (1 + \cos 2\omega t) + \ldots \quad (36)$$

The oscillator frequency may be chosen freely but should not be an integer multiple of 50 Hz or 60 Hz. The amplitude i_{osc} should be small enough to avoid averaging effects if the sample exhibits a non-linear differential resistance.

2.2 Electrical components for DC measurements

The appropriate choice of the measurement setup and of the current-sourcing and voltage-measuring instruments is determined by the range of resistivities of the materials being studied. While AC measurements are commonly used for low resistivity testing, this technique makes the results dependent on time constants and the degree to which all contacts are non-rectifying.

In many cases a quality, low-noise DC system that is capable of measuring samples with a wide range of resistivities is a good choice. For testing high resistivity materials such as lightly-doped semiconductors requires a precision low-level, low-noise current source with a high effective output resistance. For very high resistances in the 10^{12} Ω range, a system utilizing driven guards may be required. This is necessary to ensure that virtually all the current goes through the sample, not through any shunt resistance. The driven guard connection also minimizes the time constant of the measurement. Testing low resistivity samples such as heavily-doped materials or metals requires a higher-value precision current source and a very sensitive voltage-measuring instrument.

A sketch of the DC measurement setup used in this lab experiment is shown in Fig. 13. A precision low noise, low current source and a 6–1/2 digit digital multimeter are connected to the sample via a programmable matrix switch. All components can be addressed by a computer over a GPIB interface.

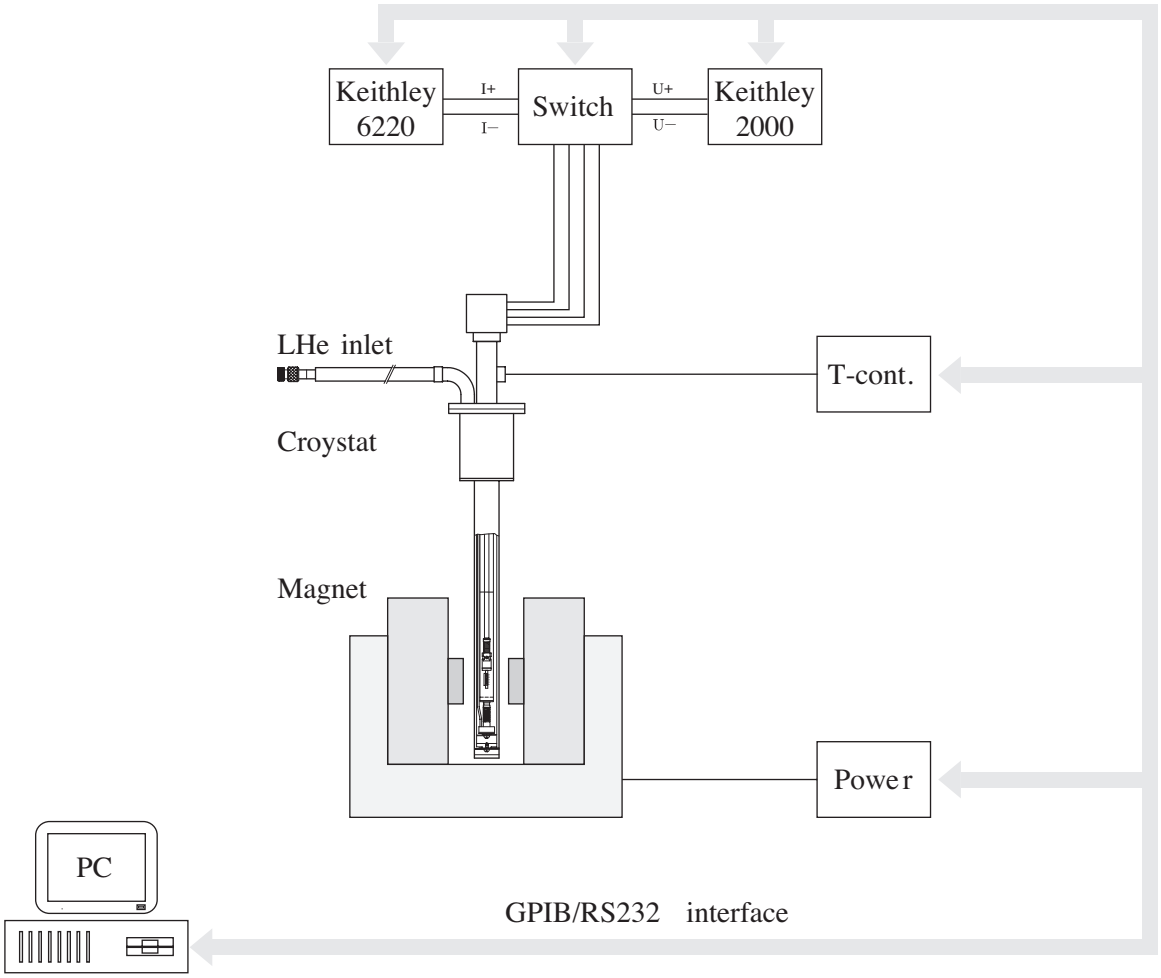

Figure 13: Measurement setup of the Hall system with DC components. A switch box is used to connect the precision current source and the digital voltmeter to the sample leads.

2.3 The cryostat

Liquid helium is continously transferred through a vacuum jacketed, superisolated flexible transfer line to a vaporizer at the bottom of the sample chamber. The liquid is then vaporized and heated to some specified temperature, and travels upwards to cool the sample and intercept the heat loads coming down the sample tube. The sample is surrounded by helium vapor, which ensures a good thermal contact to the sample. A needle valve located at the bottom of the leg of the transfer line (which goes inside the storage dewar), controls the cryogen flow to the sample mount.

Temperatures below 4.2 K are achived by reducing the pressure (using a mechanical vacuum pump) at the sample tube vent port. Temperatures above 4.2 K are obtained by sending an appropriate current through a bifilarly wound heater at the vaporizer. An additional heater is located on the sample mount. The temperature is measured with a GaAlAs diode close to the vaporizer and controlled by a PID (proportional-integral-derivative) control circuit.

Since helium is very expensive, the vapor leaving the cryostat is collected in a recovery line and liquefied in a condenser system. The liquid helium can then again be used as a cryogenic for further measurements.

In principle, this system should be a closed cycle. However, there will always be small losses when starting an experiment and when changing the sample. It is very important to limit these losses as much as possible, but without taking a risk of contaminating the helium recovery line with air, moisture or oil vapors from the mechanical pump. A piping system is used to control the flow of the helium vapor (Fig. 14). At the beginning of an experiment, the helium vapor, that is mixed with air from the cryostat, is fed to the waste air. Subsequently, only the pure helium vapor is recovered. An adjustable valve at the inlet of the rotary pump is employed to throttle the vacuum at the pumping port of the cryostat and thus control the consumption of liquid helium (together with the needle valve in the transfer line).

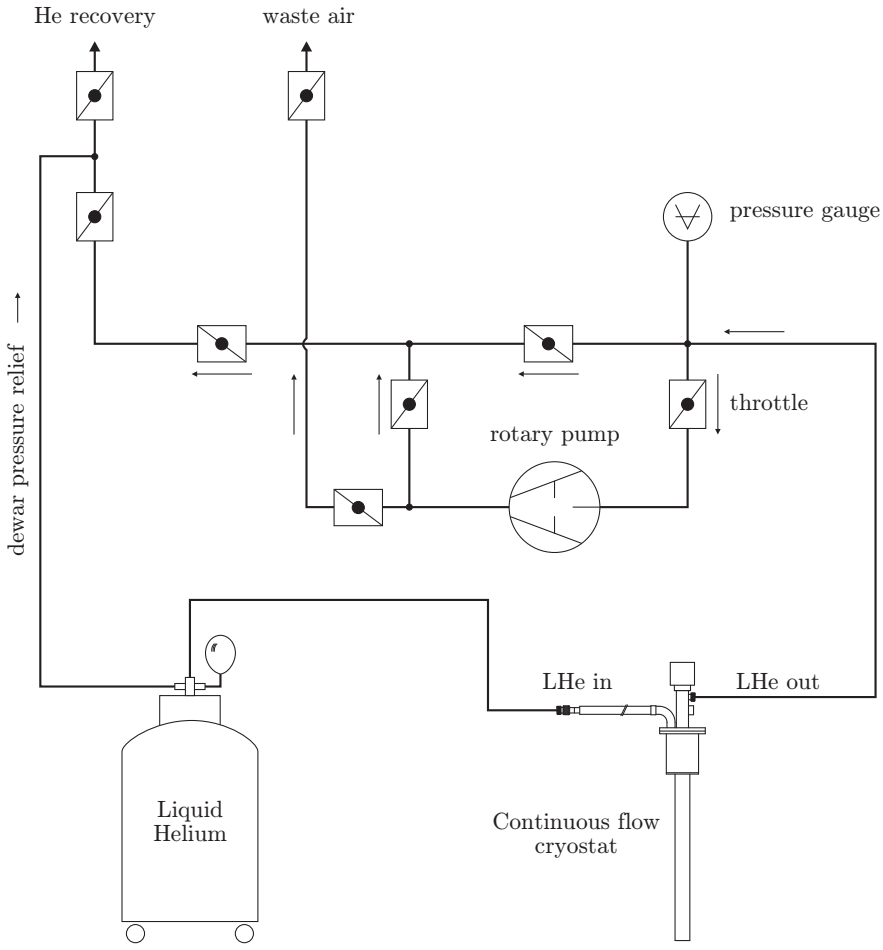

Figure 14: Layout of the helium recovery connections. A rotary pump is used to evacuate the line and exhaust any possible contaminations to the waste air, before opening the helium inlet at the cryostat. Subsequently the helium vapor from the outlet of the cryostat can be fed to the recovery line directly or through the pump.

3 Experimental procedures

At the beginning of a low temperature measurement, one should always check the sample and in particular the electrical connections. In the present cryostat, the sample exchange times are relatively short, but in more sophisticated systems it can easily take several hours to cool down and warm up again to withdraw the sample from the cryostat.

An optical microscope is available to visually inspect the sample. Subsequently, the sample has to be mounted into the sample holder and electrically contacted. Samples with hall-bar geometry in general have small area pads and need to be contacted with the help of a wire bonder. This is an apparatus that uses a small wedge and ultrasound to bond an Al-wire with a diameter of 33 μm to the sample. In the case of van der Pauw geometry, the contact pads may consist of small indium balls, to which a thin wire can be soldered manually.

The electrical connections should be checked for open circuits by means of a hand multimeter before inserting the sample into the cryostat. If the isolation vacuum in the shroud of the cryostat and in the transfer line is not in the range of 10^{-5} Torr (1 Torr = 1.33 mbar), it should be re-evacuated with a turbomolecular pumping station[1]. Now the cryostat is ready for cooldown. It should take less than 30 min to reach the lowest temperature. Always keep in mind that it is crucial to switch on the water cooling before operating the magnet!

3.1 Cooldown

When working with liquid helium one always has to wear the appropriate personal protective equipment. The minimum requirements are a face shield and cryogenic gloves!

1. Open the needle valve at the bottom of the transfer line (storage dewar leg) by turning the knurled knob one or two times (turn clockwise when viewed from top).

2. Insert the rigid leg of the transfer line into a storage dewar very slowly and tighten the brass O-ring seal nut to form a gas tight seal. Note that you will hardly be able to feel any gas exiting the transfer line bayonet.

3. Insert the male bayonet of the transfer line into the cryostat section and (hand) tighten the knurled nut on the transfer line side to ensure a good mechanical joint.

4. Close the needle valve and attach a mechanical vacuum pump to the sample tube vent/pumping port. This will evacuate the sample tube and the inner line, and provide a path for the cryogen that is free from air and moisture (the escaping vapor from the pump should be vented into the waste air line). Subsequently, the vacuum pump may be disconnected from the system and the needle valve can be

[1]When evacuation of either vacuum space is initiated, always be sure that the pressure on the pump side of the evacuation valve is lower than the pressure in that vacuum space. This is done to avoid drawing oil vapor from the pump into the vacuum space. Thus, one should not pump any vacuum space while liquid helium is passing through the inner line, since the liquid helium could cryopump to a lower pressure than the pumping station in use.

opened. The cryogen starts to flow through the inner line and the temperature in the cryostat quickly drops. The helium gas that leaves the cryostat is collected in the helium recovery line.

5. Check that the pressure inside the storage dewar is about (1 to 4) psi (1 psig = 68.9 mbar, relative to ambient atmospheric pressure), and maintain this pressure throughout this procedure. If necessary, use the rubber bladder to slightly pressurize the storage container.

3.2 Cryostat operation

For operation at 4.2 K, the flow valve should be opened just enough to maintain this temperature at the sample mount. The necessary (minimum) flow required will be a function of the heat load into the sample tube.

For temperatures above 4.2 K, send a current through the vaporizer heater and monitor the temperature of the sample mount. After a short lag, the temperature of the sample mount will increase and then stabilize at a value determined by the heater input.

It is important to make sure that helium is definitely flowing through the vaporizer prior to passing any current through this heater. If no flow exists, the vaporizer's temperature can increase very rapidly causing heater burnout or damage to the joints!

Adjustments in cryogen flow can be made at any time either to increase the cooling power, or to reduce the cryogen consumption at higher temperatures. At last, control is made through the automatic temperature controller. Please note that the sample mount temperature should never exceed 300 K.

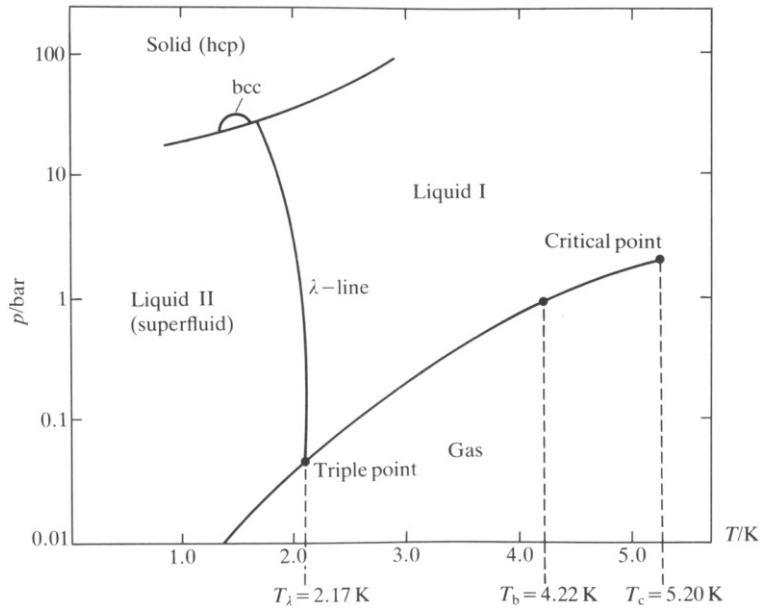

Figure 15: Phase diagram for helium (He^4). The λ-line marks the conditions under which the two liquid phases are in equilibrium (He-II is the superfluid phase). Taken from [4].

Operation below 4.2 K is achieved by reducing the pressure at the sample tube vent/pumping port with a mechanical vacuum pump (Fig. 15). The flow valve may be partially opened

(less than 1/4 turn), thus developing a pressure gradient at the needle valve and continuously transferring cold helium vapor to the sample tube. This configuration provides cooling (below 4.2 K) for extended periods of time. Lower temperatures can be achieved by filling the sample tube, closing the flow valve and then reducing the pressure on top of this helium. The low temperature will be maintained until all the superfluid helium is depleted from the sample tube. A slightly higher temperature will be reached if the needle valve is throttled to continuously replenish the liquid helium in the sample tube.

Upon the completion of the experiment, the needle valve of the transfer line should be closed. The storage dewar should then be depressurized by opening the valve to the helium recovery, and the transfer line should be removed in order to reduce the heat input into the liquid inside the dewar.

4 Experiment

4.1 Van der Pauw measurement

Make a room temperature van der Pauw measurement on a square sample (2DEG in an AlGaN/GaN heterostructure) at different magnetic fields up to about 0.5 T. Remember to adjust the sample perpendicular to the magnetic field.

- Calculate the carrier concentration and the mobility according to the procedure described in Sec. 1.5.
- Plot the magnetic field dependence of the individual Hall voltages and comment on the result.

4.2 Classical Hall-Effect

Mount the bar-type sample, which is an InGaAs/InP based 2DEG structure (as described in Fig. 3b), and ensure that all the sample contacts exhibit ohmic behavior. Make an initial measurement at room temperature and then cool down the cryostat. Measure the temperature dependent mobility and carrier concentration. Remember to adjust the sample perpendicular to the magnetic field.

- Analyse the residuals of the linear regressions, that were performed to determine the Hall resistivity and the longitudinal resistivity: Are the deviations stochastic or systematic? What can be concluded from this analysis?
- Plot the carrier concentration as a function of temperature. Can the observed behaviour be described by thermal activation of carriers? If so, what is the corresponding activation energy?
- Plot the calculated mobility against temperature and determine the temperature exponent in the higher temperature range – including the confidence interval. Compare your result to the description in Sec. 1.1.

4.3 Quantum Hall-Effect

The same sample used in Sec. 4.2 has also been characterized at high magnetic fields in a commercial setup (Quantum Design - Physical Property Measurement System, PPMS®). At low temperatures, one can clearly observe quantum Hall plateaus and Shubnikov-de-Haas oscillations. The corresponding dataset is provided for further analysis.

- Plot the Hall resistance against magnetic field and determine the value of the plateaus in units of h/e^2. Compare your results to the theoretical values for suitable filling factors. Comment on significant deviations, if any.
- Plot the longitudinal resistivity against magnetic field and discuss the observed behavior with respect to the theoretical prediction of Shubnikov-de-Haas oscillations.

- Determine the sheet carrier concentration n_e from the periodicity of the Shubnikov-de-Haas oscillations in $(1/B)$ and compare the result to the classical Hall measurement analysis of Sec. 4.2.

Guidelines for the preparation of the report

- Please give a *concise* summary of the physical background. The concepts and equations that are necessary for the subsequent analysis and discussion should be presented in a clear and logical way. Refer to the literature for any further details.
- Please discuss all your results *directly*. It is not recommended to shift the discussion of the various measurement tasks into a separate chapter.
- Always choose a meaningful way to plot your data. All graphs should be properly scaled and labeled.
- The report may be prepared either in German or in English.

Additional documentation

A folder with additional documentation is available for this lab experiment.
Please contact the responsible tutor for any details.

- Original papers by E. D. Hall and L. J. van der Pauw
- Janis Research Company: cryostat layout and sample wiring
- Lake Shore: PID control (excerpt from user's manual)
- Material safety data sheet for liquid helium

References

[1] H. Ibach and H. Lüth. *Festkörperphysik*. Springer, 1999.

[2] E. H. Hall. On a new action of the magnet on electric currents. *American Journal of Mathematics*, 2:287–292, 1879.

[3] L. J. van der Pauw. A method of measuring specific resistivity and hall effect of discs of arbitrary shape. *Philips Research Reports*, 13:1–9, 1958.

[4] P. W. Atkins. *Physical Chemistry*. Oxford University Press, 1990.

[5] S. Datta. *Electronic Transport in Mesoscopic Systems*. Cambridge University Press, 1995.

[6] T. Heinzel. *Mesoscopic Electronics in Solid State Nanostructures*. Wiley-VCH, 2007.

[7] P. Phillips. *Advanced Solid State Physics*. Westview Press, 2003.

[8] K. von Klitzing. The quantized Hall effect. *Reviews of Modern Physics*, 58:519–531, 1986.

[9] K. von Klitzing, G. Dorda and M. Pepper. New Method for High-Accuracy Determination of the Fine-Structure Constant Based on Quantized Hall Resistance. *Physical Review Letters*, 45:494–497, 1980.

[10] D. C. Tsui, H. L. Stormer and A. C. Gossard. Two-Dimensional Magnetotransport in the Extreme Quantum Limit. *Physical Review Letters*, 48:1559–1562, 1982.

[11] J. H. Davies. *The Physics of Low-Dimensional Semiconductors*. Cambridge University Press, 1998.

[12] M. Janßen, O. Viehweger, U. Fastenrath and J. Hajdu. *Introduction to the Theory of the Integer Quantum Hall Effect*. Wiley-VCH, 1994.